IJE TRANSACTIONS A: Basics Vol. 27, No. 1, (January 2014) 91-100

International Journal of Engineering

Journal Homepage: www.ije.ir

A New Method for Root Detection in Minirhizotron Images: Hypothesis Testing Based on Entropy-based Geometric Level Set Decision

S. V. Shojaedini, M. Heidari*

Department of Electrical Engineering, Iranian Research Organization for Science and Technology , Tehran-Iran

PAPER INFO

Paper history:
Received 10 June 2013
Received in revised form 27 August 2013
Accepted 14 September 2013

Keywords:
Root Detection
Minirhizotron Images
Hypothesis testing
Entropy
Geometric Level Set

ABSTRACT

A new method is introduced here for root detection in minirhizotron images for root investigation. In this method, a hypothesis testing framework is defined first to separate roots from background and noise. Then, the correct roots are extracted by an entropy-based geometric level set decision function. Performance is evaluated on real captured images in two different scenarios. In the first scenario, images contain several roots while the second scenario belongs to no-root images, which increases the chance of false detections. The results demonstrate better capability of the proposed method in root detection compared to the present approaches in all the cases investigated. Furthermore, it can be shown that better detection of roots in the proposed algorithm not only does not lead to extracting more false particles, but also it decreases rate of false detections compared to the existing algorithms.

doi: *10.5829/idosi.ije.2014.27.01a.12*

1. INTRODUCTION

The root morphological traits are one of the most important parameters for monitoring growth procedure of many plants [1]. Therefore, some details of root morphology such as its size and distribution must be frequently observed under natural growing conditions [2]. The main difficulty in such investigation is that the roots are included in the soil and cannot easily be separated from it.

For many years the root parameters have been studied by utilizing soil core sampling methods [3]. These methods can provide precise information about root parameters. However, they are destructive and time consuming [3, 4].

Rhizotrons are high-technology equipment for root observation under natural conditions without soil core sampling. They utilize transparent walls and specially designed microscopes for extracting details of root morphology [5]. Rhizotron is an expensive equipment, so it is supplanted by minirhizotron which is a combination of camera and transparent plastic tube. This set is buried at an angle in soil near the plant, so the minirhizotron images just represent a small cross-section through the soil. As the root often has a spatial distribution, a large number of minirhizotron images may be required to study all of the root parameters. The most critical part of root investigation by using these images is to extract root completely from images which leads to accurate estimation of root parameters [6, 7].

Several methods have been used for root detection in minirhizotron images with the oldest one being manual detection by an expert. Unfortunately, this method is labor-intensive and its performance is degraded by human errors. Therefore, the automated methods have been substituted for processing these images [8].

The main challenges which limit the performance of the automated methods are: the low contrast of captured images, presence of bright background objects which may be detected as roots, and finally the possible changing brightness at different parts of root which may be interpreted as root splitting [9]. Several approaches have been proposed to solve automatic root detection problems. Thresholding is one the most popular methods for image segmentation [10], so some researchers used several types of global and local

*Corresponding Author Email: shojadini@irost.ir (S. V. Shojaedini)

thresholding techniques for root detection in minirhizotron images. Unfortunately, these methods are unable to extract roots accurately because background objects have the same intensity distribution as the roots and the resulting histograms do not possess the desired bimodal [11, 12]. Other methods try to obtain the bimodal histograms by improving the contrast in images. For example the contrast stretching algorithm ensures that only a few root pixels and some bright background objects are left in the intermediate gray level. This idea is not suitable for large number of minirhizotron root images taken from various backgrounds and recorded with different luminance and exposure levels [13]. Another group of methods include region- based root detection. The main limitation of these methods is their low detection rate due to the low contrast of roots and background soil in minirhizotron images [14].

Some approaches utilize geometric features of roots, to reduce detection of no-root objects (i.e., false positives). The minimum root length (MRL) method is a suitable example for such methods. This method is based on the assumption that bright objects with skeletons shorter than the experimentally determined MRL must be considered as background. Although this method may remove some no-root objects, but some short roots may be eliminated by such a filter and this method cannot completely detect all roots [15].

In other investigations artificial neural networks have been utilized to identify roots in minirhizotron images. This approach provides excellent results when applied for identification of roots which the neural network has been trained with. However there is a considerable decrease in detection rate when the neural network is applied to other images on which it had not been trained [16].

Some recent methods utilize the local entropy followed by image morphologic operators to separate roots from background [17]. Despite considerable potential of these approaches in extracting some parts of roots, these techniques lead to fragmented roots. Furthermore, simple morphologic operators cannot prune background pixels which are included as a part of roots (e.g. false detections).

In this paper a new method is introduced which detects roots in minirhizotron images by using entropy based level-set segmentation. In the proposed method, the dependency of each pixel in captured image to root or background is modeled by using hypothesis testing framework. To assign the pixel to one of the above hypotheses, a decision function is constructed using an entropy-based geometric level set model. Utilizing level set concept enables the proposed algorithm to detect roots in low contrast minirhizotron images without splitting them unlike the existing methods. This leads to reduced detection of no-root objects without losing correct roots.

The paper is organized as follows. In Section 2, the proposed algorithm is introduced including hypothesis testing framework, estimating entropy from gray level co-occurrence matrix and constructing the energy function which leads to extract edge-based level set. In Section 3, the performance of the proposed method is evaluated in two different scenarios based on real minirhizotron images. In Section 4, the results obtained from the experiments are compared with those of the existing methods using their effective parameters. Conclusion is presented in the last section of the paper.

2. MATHEMATICAL MODEL

Suppose I as a minirhizotron image that contains root, soil and several underground particles which the two latter parameters is called background in this article. For each pixel of I it can be written:

$$I_{lj} = I(l, j) \quad 1 \le l \le L \quad 1 \le j \le J \tag{1}$$

In the above equation, I_{lj} is brightness of a pixel in I which is located in row l and column j, respectively. Also, L and J are the image sizes. Dependence of the pixel I_{lj} to the background and noise (H_0) or its dependence to the root (H_1) is determined defining hypothesis testing Equation (2):

$$\begin{cases} H_0: & I_{lj} = \left| c_{lj} + n_{lj} \right| \\ H_1: & I_{lj} = \left| r_{lj} + c_{lj} + n_{lj} \right| \end{cases} \tag{2}$$

In the above equation, r_{lj}, c_{lj} and n_{lj} show the root, background and noise components in I_{lj} respectively. Assume that I has N gray levels denoted by $\beta = \{0,1,2,...,N-1\}$ which constructs 1-D histogram of I. But, this 1-D histogram neglects the correlation among gray levels of root and background which is vital in segmentation of I. In order to resolve this problem, the co-occurrence matrix is introduced which is a square matrix as: $W = [w_{kz}]_{N*N}$ in which w_{kz} is the numbers of transitions between all pairs of gray levels in β. The above parameter is defined as [18, 19]:

$$w_{kz} = \sum_{l=1}^{L} \sum_{j=1}^{J} \tau_{lj} \tag{3}$$

In which

$$\tau_{lj} = \begin{cases} 1 & if\ I_{lj} = k \ \ and \ \ I_{l+1,j} = z \\ 1 & if\ I_{lj} = k \ \ and \ \ I_{l,j+1} = z \\ 0 & otherwise \end{cases} \tag{4}$$

The transition probability from gray level k to gray level z is obtained as:

$$g_{kz} = \frac{w_{kz}}{\sum_{k'=0}^{N-1}\sum_{z'=0}^{N-1} w_{k'z'}} \tag{5}$$

Let T be a threshold used to separate root from other particles in minirhizotron image I. Therefore, it partitions co-occurrence matrix into four quadrants as A_1, A_2, A_3 and A_4. These four quadrants can be clustered into two classes. Let pixels with gray levels above the threshold be assigned to the root and those equal to or below the threshold ,to the background. Therefore, A_1 and A_3 show local transitions within background and root, which are called local quadrants. The quadrants A_2 and A_4 represent joint transitions across boundaries between background and root which are called joint quadrants. The probability of each quadrant is:

$$\begin{aligned} G_{A_1}^T &= \sum_{k=0}^{T}\sum_{z=0}^{T} g_{kz} & G_{A_3}^T &= \sum_{k=T+1}^{N-1}\sum_{z=0}^{T} g_{kz} \\ G_{A_2}^T &= \sum_{k=0}^{T}\sum_{z=T+1}^{N-1} g_{kz} & G_{A_4}^T &= \sum_{k=T+1}^{N-1}\sum_{z=T+1}^{N-1} g_{kz} \end{aligned} \tag{6}$$

Suppose the threshold T to be applied to the original image I and lead to processed image I'. Now, the transition probabilities of I are shown as $G=[g_{kz}]_{N*N}$, and for the I' as $X^T=[x^T{}_{kz}]_{N*N}$, where $x^T{}_{kz}$ has the similar definition as g_{kz}. The second-order cross-entropy of the above gray-level transition probabilities is defined as [20]:

$$E(G, X^T) = \sum_{k=0}^{N-1}\sum_{z=0}^{N-1} g_{kz} \log \frac{g_{kz}}{x_{kz}^T} \tag{7}$$

The above entropy is used to measure the information distance between the original image I and the processed (e.g. thresholded) image I'. Therefore, the smaller this entropy is, the closer the two images are in terms of their probability distributions. Based on this fact, it can be concluded that minimization of $E(G, X^T)$ over T generates I' in such way that best matches I. Let all gray levels above T be called $\beta_1 = \{T+1, T+2, ..., N-1\}$ and all gray levels equal to or below T called $\beta_0 = \{0,1,...,T\}$. So, β_1 and β_0 are partitioned sets of β that had been introduced before. Assuming that gray levels in β_1 and β_0 are uniformly distributed in their respective regions, the resulting x_{kz}^T for each quadrant can be found by [21, 22]:

$$\begin{aligned} x_{kz|A_1}^T &= \frac{G_{A_1}^T}{(T+1)(T+1)}, \quad \forall k, z \in \beta_0 \\ x_{kz|A_2}^T &= \frac{G_{A_2}^T}{(T+1)(N-T-1)}, \forall k \in \beta_0, z \in \beta_1 \\ x_{kz|A_3}^T &= \frac{G_{A_3}^T}{(N-T-1)(N-T-1)}, \forall k \in \beta_1, z \in \beta_1 \\ x_{kz|A_4}^T &= \frac{G_{A_4}^T}{(N-T-1)(T+1)}, \forall k \in \beta_1, z \in \beta_0 \end{aligned} \tag{8}$$

where $G_{A_1}^T$, $G_{A_2}^T$, $G_{A_3}^T$ and $G_{A_4}^T$ were defined by (6). For each selected T, $x_{kz|A_1}^T$, $x_{kz|A_2}^T$, $x_{kz|A_3}^T$ and $x_{kz|A_4}^T$ are constants in each individual quadrant and they only depend upon the quadrants they belong to. To optimize Equation (7) which leads to obtaining the best value of T, firstly it is expanded as:

$$E(G, X^T) = E'([g_{kz}]) - \sum_{k=0}^{N-1}\sum_{z=0}^{N-1} g_{kz} \log x_{kz}^T = E'(G) - E''(T) \tag{9}$$

In the above equation, $E'(G)$ is the entropy of the probability matrix G and is independent of T, so $E''(T)$ is only threshold-dependent part of entropy. As mentioned before, the best T is the one that yields the smallest value of $E(G, X^T)$. However, minimization of $E(G, X^T)$ in Equation (9) is equivalent to maximizing the second term of the right-hand-side of this equation, which can be further reduced to:

$$\begin{aligned} E''(T) = {} & G_{A_1}^T.\log(x^T{}_{kz|A_1}) + G_{A_2}^T.\log(x^T{}_{kz|A_2}) + \\ & G_{A_3}^T.\log(x^T{}_{kz|A_3}) + G_{A_4}^T.\log(x^T{}_{kz|A_4}) \end{aligned} \tag{10}$$

Therefore, the threshold value T that maximizes (10) is found as:

$$T = \arg\left\{ \min_{T \in \beta} E''(T) \right\} \tag{11}$$

Let the result of thresholding by T be a processed image I' which is defined as:

$$\begin{cases} I'_{ij} = I_{ij} & I_{ij} > T \\ 0 & otherwise \end{cases} \tag{12}$$

Let the edge indicator d be defined for the thresholded image I' as:

$$d = \frac{1}{1 + \nabla D_\sigma * I'^2} \tag{13}$$

where D_σ is a Gaussian kernel with a standard deviation σ. The convolution term $\nabla D_\sigma * I'^2$ acts as smoothing filter for noise reduction. The edge indicator d usually takes smaller values at object boundaries than at other locations.

Supposing ϕ as the level set function (LSF) on I', the energy function can be defined as:

$$O(\phi) = \mu R_p(\phi) + \lambda \eta_d(\phi) + \alpha \psi_d(\phi) \quad (14)$$

in which $\mu > 0$ is a constant and $R_p(\phi)$ is the level set regularization term defined as:

$$R_p(\phi) = \int_{I'} p(|\nabla \phi|) dX \quad (15)$$

where $p(|\nabla \phi|)$ is potential function which is defined as:

$$p(|\nabla \phi|) = \frac{1}{2} \int_{I'} (|\nabla \phi| - 1)^2 \, dX \quad (16)$$

Based on Equations (15) and (16), it is clear that $R_p(\phi)$ has a minimum point at $|\nabla \phi| = 1$.

In the second and third terms of Equation (14), $\lambda > 0$ and $\alpha \in R$ are the coefficients of the energy functions $\eta_d(\phi)$ and $\psi_d(\phi)$ which are defined as:

$$\eta_d(\phi) = \int_{I'} d\delta(\phi) \nabla \phi dX \quad (17)$$

$$\psi_d(\phi) = \int_{I'} dH(-\phi) dX \quad (18)$$

where $\delta(.)$ and $H(.)$ are the Dirac and the Heaviside functions, respectively. Using these functions, the energy $\eta_d(\phi)$ computes the line integral of d along the zero level contour of ϕ. This energy is minimized when the zero level contour of ϕ is located at the object boundaries [23].

The energy functional $\psi_d(\phi)$ computes a weighted area of the region $I'_\phi = \{s : \phi(s) < 0)\}$ and is introduced to speed up the motion of the zero level contour in the level set evolution process, which is necessary when the initial contour is placed far away from the desired object boundaries.

In this paper, we use LSFs that take negative values inside the zero level contour and positive values outside. In this case, if the initial contour is placed outside the object, the coefficient α in the weighted area term should be positive, so that the zero level contours can shrink in the level set evolution. If the initial contour is placed inside the object, this coefficient should take negative value to expand the contour.

In practice $\delta(.)$ and $H(.)$ in Equations (17) and (18) are approximated by the following smooth functions [24, 25]:

$$\delta_\varepsilon(\phi) = \begin{cases} \frac{1}{2\varepsilon}\left[1 + \cos(\frac{\pi\phi}{\varepsilon})\right] & \phi \le \varepsilon \\ 0 & \phi > \varepsilon \end{cases} \quad (19)$$

$$H_\varepsilon(\phi) = \begin{cases} \frac{1}{2}\left[1 + \frac{\phi}{\varepsilon} + \frac{1}{\pi}\sin(\frac{\pi\phi}{\varepsilon})\right] & \phi \le \varepsilon \\ 1 & \phi > \varepsilon \\ 0 & \phi < -\varepsilon \end{cases} \quad (20)$$

Substituting above functions in main Equation (14), energy is approximated by:

$$O_\varepsilon(\phi) = \mu \int_{I'} p(|\nabla \phi|) dS + \lambda \int_{I'} d\delta_\varepsilon(\phi) \nabla \phi dS + \alpha \int_{I'} dH_\varepsilon(-\phi) dS \quad (21)$$

This energy can be minimized by solving the following gradient flow:

$$\frac{\partial \phi}{\partial t} = \mu . div(\theta_p(|\nabla \phi|) \nabla \phi) + \lambda \delta_\varepsilon(\phi) . div(d \frac{\nabla \phi}{|\nabla \phi|}) + \alpha d \delta_\varepsilon(\phi) \quad (22)$$

where $div(.)$ is divergence operator and θ_p is a function defined as:

$$\theta_p(|\nabla \phi|) = \frac{p'(|\nabla \phi|)}{|\nabla \phi|} \quad (23)$$

where $p'(|\nabla \phi|)$ is derivative of function $p(|\nabla \phi|)$ which has been introduced in Equation (16).

Now dependence of a pixel to background and noise (H_0) or to root (H_1) is determined by combining Equations (2) and (22) as:

$$\begin{cases} H_0 : \quad i_{lj} \notin \phi \Rightarrow i_{lj} = |c_{lj} + n_{lj}| \\ H_1 : \quad i_{lj} \in \phi \Rightarrow i_{lj} = |r_{lj} + c_{lj} + n_{lj}| \end{cases} \quad (24)$$

3. TESTS AND RESULTS

The proposed algorithm was applied to real data. The data set was several minirhizotron images where half of them contained various types of roots and the remaining half were no-root images composed of background objects or dead roots. Table 1 depicts some important parameters corresponding to images (e.g. number, contrast and size) and some parameters of roots which these images belong to (e.g. type, length and width of roots). More detail about the dataset can be found in [17]. The proposed method was implemented using Matlab 2009. Additionally, Entropy Thresholding Algorithm (ETA) [17], Minimum Root Length (MRL) [15], Region Based Root Detection (RBRD) [14] and Histogram Thresholding Algorithm (HTA) [12] were implemented to compare with the proposed algorithm. For brevity some results of the proposed, ETA and HTA methods are graphically showed in this part of article, but the complete statistics of the test results will be

discussed in part 4. The captured videos were first processed using manual detection to obtain a ground-truth detection to compare the automatic methods with. Then roots were detected by applying the proposed and other algorithms. Finally, performance of each algorithm was determined by comparing its results with manual detection. The complete extraction of roots is essential to compute their parameters, so, each detection was considered as a correct root only if at least 90% of its pixels had been extracted same as manual detection.

3. 1. First Scenario In the first scenario the implemented algorithms were applied on images which had been captured from root-contained scenes. Figures (1-b), (1-c) and (1-d) show results by utilizing three algorithms on image shown in Figure (1-a). It can be seen in (1-b) that the HTA has extracted the correct root but with great number of extra pixels (note bottom of root);, also this algorithm has extracted a completely false root. Figure (1-c) shows that result obtained from ETA. This result contains the partitioned correct root as two separated roots and furthermore some parts of root have become loose The result of applying the proposed method has been shown in Figure (1-d) which implies the complete extraction of correct root neither with false detections nor splitting effect.

Figure (2) shows another type of results. Figure (2-b) shows that the HTA has extracted one of totally two roots existing in Figure (2-a). Note that this root is extracted with some extra pixels and so it may cause some errors in extracting geometric features of root. As shown in (2-c) ETA also has extracted both roots, but the second root has been extracted in fragmented parts. Although (2-d) shows that the proposed algorithm has extracted both roots better than the other two algorithms, but still the second root has been detected incompletely.

3. 2. Second Scenario The existence of some bright background objects which can be detected as roots is one of the challenges in root detection problem. Therefore, in this scenario those images were examined which have been captured from no-root scenes. An example for such images is shown in Figure (3-a). Figure (3-b) shows the result which has been obtained from processing (3-a) by HTA with a false detection. But as shown in (3-c) and (3-d), ETA and the proposed algorithm have had no false detections.

4. PERFORMANCE MEASURES

Real data were analyzed using ETA, MRL, RBRD, HTA and the proposed method and the results were compared with manual detection ones using two standard parameters. The first parameter was defined as the probability of correct association of pixels to valid roots which is called the probability of detection as:

$$P_D = P(I_{ij} \in \phi \mid H_1) \tag{25}$$

This parameter was estimated as:

$$P_D = (1 - \frac{\sum_{k=1}^{total\,images} Missed\ roots\ in\ image\ k}{total\ images \times number\ of\ roots}) * 100 \tag{26}$$

The second evaluation parameter was the probability of associating the pixels to incorrect roots which is called false alarm probability:

$$P_{fa} = P(I_{ij} \in \phi \mid H_0) \tag{27}$$

This parameter was estimated as:

$$P_{fa} = \frac{\sum_{k=1}^{total\,images} false\ roots\ in\ image\ k}{total\ images \times number\ of\ roots} * 100 \tag{28}$$

Using the mentioned parameters, changes of detection rate versus false detection rate (e.g. ROC curve) have been obtained for both scenarios and all examined methods as shown in Figure (4). This figure shows the superiority of the proposed method compared to other four examined algorithms. For better interpretation of results, $P_{fa} = 5\%$ and $P_D = 90\%$ were considered as typical acceptable values for false detection and detection probabilities and Table 2 was constructed from Figure (4). The performance of algorithms may be compared using other arbitrary thresholds for acceptable P_{fa} and P_D by using Figure (4) in the same manner.

As shown in Table 2, the proposed algorithm has achieved detection rates of 19%, 24%, 28% and 42% better than ETA, MRL, RBRD and HTA methods respectively, versus 5% of false detection. Also, this table shows that the detection rate of the proposed algorithm reaches 90% without any false detection, that is 20% ,35% , 40% and 45% better than false alarm values which have been obtained for MRL, RBRD and HTA for the same detection rate.

TABLE 1. Specifications of examined minirhizotron images and roots

Specification of Images	Value	Specification of Roots	Value
Number of tested images	100 frames	Plant Species	Magnolia and Peach
Average contrast	19%	Min and Max length of roots	60 , 490 pixels
Frame size (pixels)	480*640 pixels	Min and Max width of roots	12 , 33 pixels

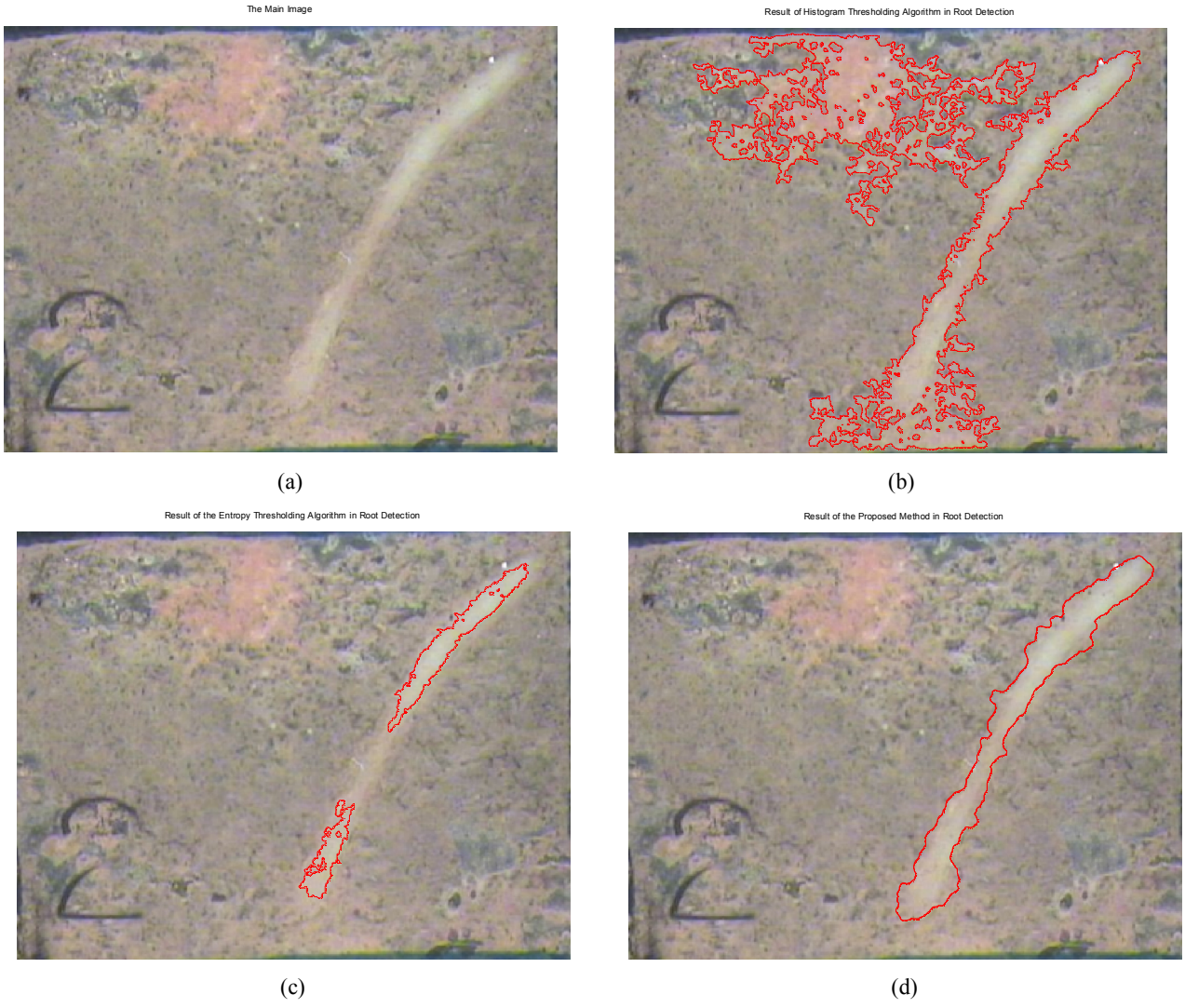

Figure 1. (a) - A One-Root hand-labeled minirhizotron image and detection results of (b) - HTA , (c)- ETA and (d)-The Proposed Algorithm

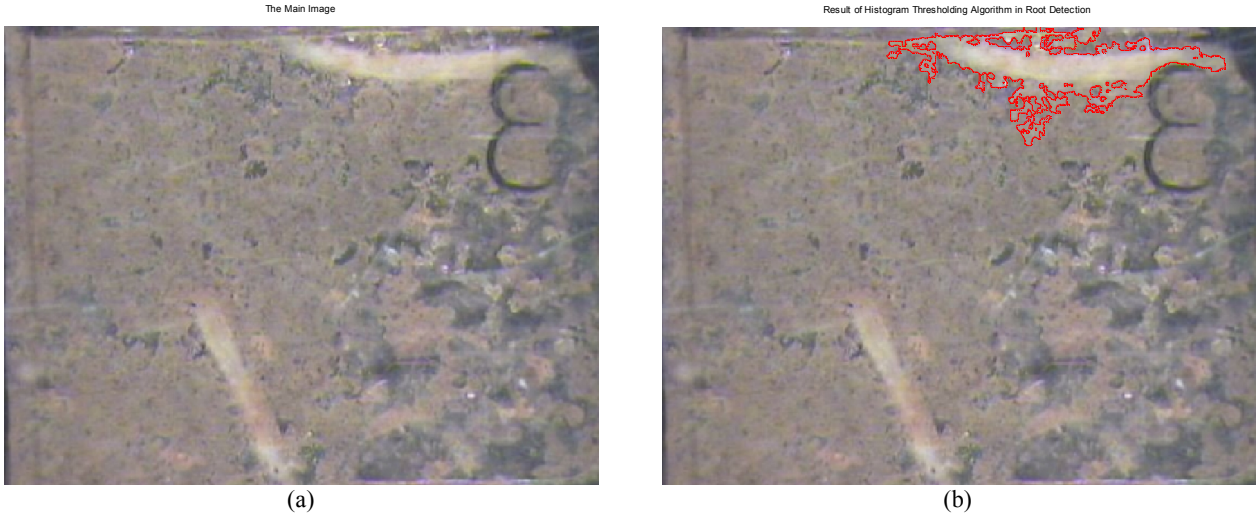

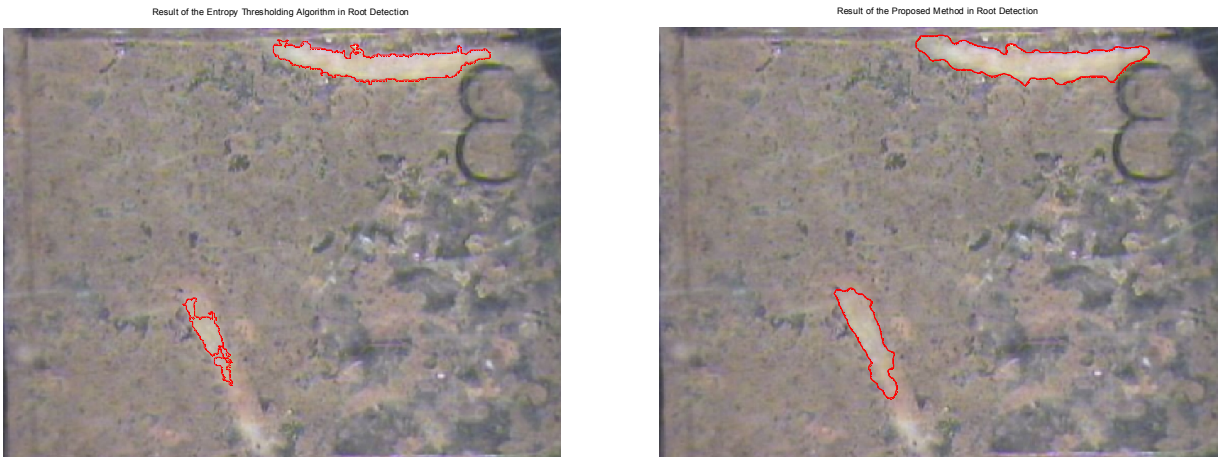

(c) (d)

Figure 2. (a) - A Two-Root hand-labeled minirhizotron image and detection results of (b) - HTA ,(c)- ETA and (d)-The Proposed Algorithm

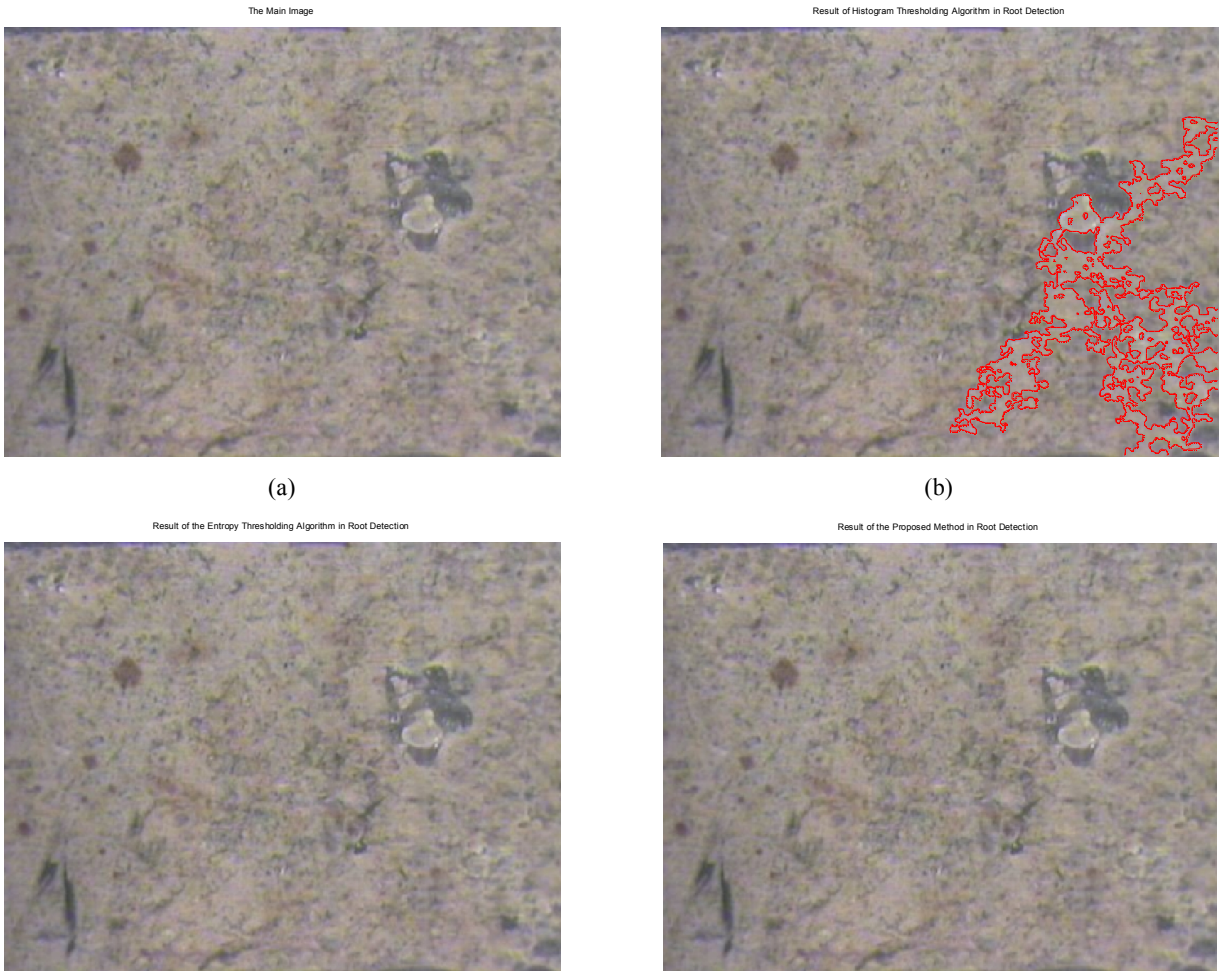

(a) (b)

(c) (d)

Figure 3. (a) - A No-Root hand-labeled minirhizotron image and detection results of (b)- HTA , (c)- ETA and (d)-The Proposed Algorithm

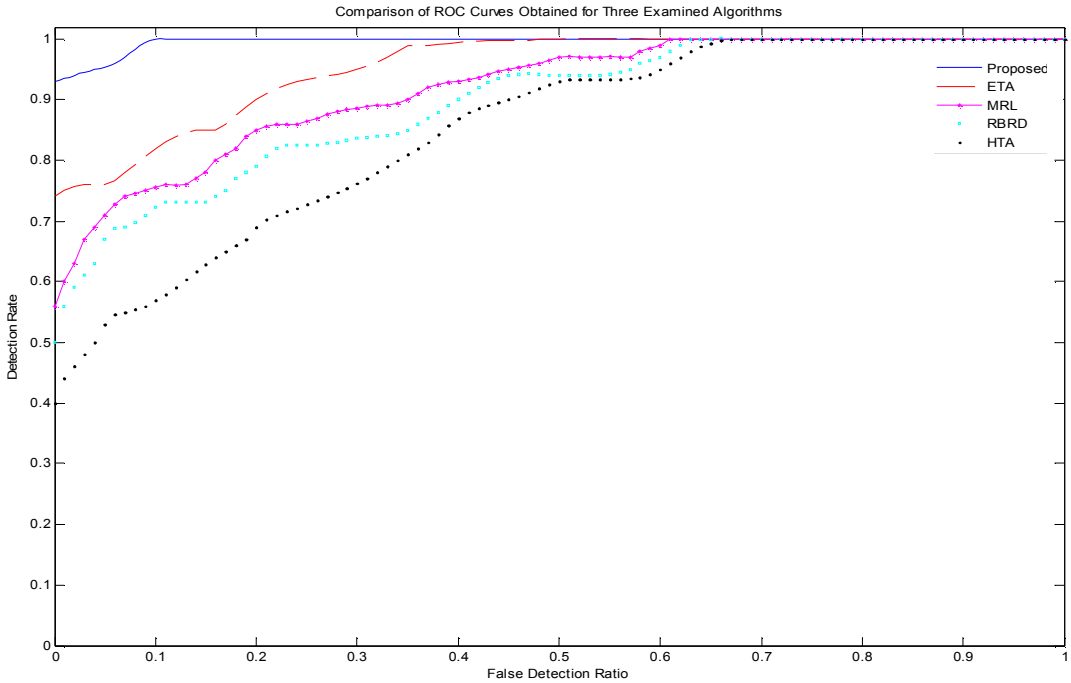

Figure 4. ROC curves obtained for the proposed (solid line-blue), ETA (dashed line-red), MRL (square line- magenta), RBRD (square -cyan) and HTA (dotted- black) algorithms

TABLE 2. Comparison of the performances of examined algorithms

Examined Methods	Parameters	
	P_D	P_{fa}
Proposed	0.95	0
ETA	0.76	0.2
MRL	0.71	0.35
RBRD	0.67	0.40
HTA	0.53	0.45

5. CONCLUDING REMARKS

In this paper a new method was introduced for automated root detection in minirhizotron images. The proposed method first modeled the dependence of each pixel to root or background in the hypothesis testing framework. Then, the correct hypotheses was determined by minimizing the energy function of an entropy-based geometric level set model.

To evaluate the performance of the proposed algorithm, two scenarios were considered based on real captured images which may or may not contain different roots. The performance of the proposed algorithm was compared with ETA, MRL, RBRD and HTA in terms of detection and false alarm rates. Numerical comparison showed better performance of the proposed algorithm in root detection compared to the other. From the inspection of the ROC curves, it was observed that the proposed algorithm has extracted roots at least 19% more than the best of all the other examined methods in presence of a typically low false detection rate equal to 5%. Furthermore, it was shown that false detection rate of the proposed algorithm was at least 20% less than the best of other examined methods considering the minimum acceptable detection rate of 90%. These results demonstrated that better root detection capability obtained by the proposed algorithm not only has not increased false detections, but has improved false alarm rate instead. Consequently, it can be concluded that the proposed method may be used as a suitable alternative for detecting roots in minirhizotron images which have poor contrast and low SNR.

6. REFERENCES

1. Hodge, A., Berta, G., Doussan, C., Merchan, F. and Crespi, M., "Plant root growth, architecture and function", ***Plant and Soil***, Vol. 321, No. 1-2, (2009), 153-187.
2. Genc, Y., Huang, C. Y. and Langridge, P., "A study of the role of root morphological traits in growth of barley in zinc-deficient soil", ***Journal of Experimental Botany***, Vol. 58, No. 11, (2007), 2775-2784.
3. Himmelbauer, M., "Estimating length, average diameter and surface area of roots using two different image analyses systems", ***Plant and Soil***, Vol. 260, No. 1-2, (2004), 111-120.
4. Ping, X., Zhou, G., Zhuang, Q., Wang, Y., Zuo, W., Shi, G., Lin, X., and Wang, Y., "Effects of sample size and position from

monolith and core methods on the estimation of total root biomass in a temperate grassland ecosystem in inner mongolia", ***Geoderma***, Vol. 155, No. 3, (2010), 262-268.

5. Silva, D. D. and Beeson, R. C., "A large-volume rhizotron for evaluating root growth under natural-like soil moisture conditions", ***HortScience***, Vol. 46, No. 12, (2011), 1677-1682.
6. Hendricks, J. J., Hendrick, R. L., Wilson, C. A., Mitchell, R. J., Pecot, S. D., and Guo, D., "Assessing the patterns and controls of fine root dynamics: An empirical test and methodological review", ***Journal of Ecology***, Vol. 94, No. 1, (2006), 40-57.
7. Munoz-Romero, V., Benítez-Vega, J., López-Bellido, L. and López-Bellido, R. J., "Monitoring wheat root development in a rainfed vertisol: Tillage effect", ***European Journal of Agronomy***, Vol. 33, No. 3, (2010), 182-187.
8. Zeng, G., Birchfield, S. T. and Wells, C. E., "Automatic discrimination of fine roots in minirhizotron images", ***New Phytologist***, Vol. 177, No. 2, (2008), 549-557.
9. Andrén, O., Elmquist, H. and Hansson, A.-C., "Recording, processing and analysis of grass root images from a rhizotron", ***Plant and Soil***, Vol. 185, No. 2, (1996), 259-264.
10. Hassanpour, H. and Yousefian, H., "An improved pixon-based approach for image segmentation", ***International Journal of Engineering-Transactions A: Basics***, Vol. 24, No. 1, (2010), 25.
11. Smit, A. L., "Root methods: A handbook", Springer, (2000).
12. Vamerali, T., Ganis, A. and Mosca, G., "Methods for thresholding minirhizotron root images", ***International Symposium of Root Research and Applications, Vienna, Austria,***, (2009), 1-2.
13. Vamerali, T., Ganis, A., Bona, S. and Mosca, G., "An approach to minirhizotron root image analysis", ***Plant and Soil***, Vol. 217, No. 1-2, (1999), 183-193.
14. Erz, G. and Posch, S., A region based seed detection for root detection in minirhizotron images, in Pattern recognition., Springer. (2003) 482-489.
15. Vamerali, T., Guarise, M., Ganis, A., Bona, S. and Mosca, G., Analysis of root images from auger sampling with a fast procedure: A case of application to sugar beet, in Roots: The dynamic interface between plants and the earth., Springer. (2003), 387-397.
16. Nater, E. A., Nater, K. D. and Baker, J. M., "Application of artificial neural system algorithms to image analysis of roots in soil, i. Initial results", ***Geoderma***, Vol. 53, No. 3, (1992), 237-253.
17. Zeng, G., Birchfield, S. T. and Wells, C. E., "Detecting and measuring fine roots in minirhizotron images using matched filtering and local entropy thresholding", ***Machine Vision and Applications***, Vol. 17, No. 4, (2006), 265-278.
18. Baraldi, A. and Parmiggiani, F., "An investigation of the textural characteristics associated with gray level cooccurrence matrix statistical parameters", ***Geoscience and Remote Sensing, IEEE Transactions on***, Vol. 33, No. 2, (1995), 293-304.
19. Kekre, H., Thepade, S. D., Sarode, T. K. and Suryawanshi, V., "Image retrieval using texture features extracted from glcm, lbg and kpe", ***International Journal of Computer Theory and Engineering***, Vol. 2, No. 5, (2010), 1793-8201.
20. Horng, M.-H., "Multilevel minimum cross entropy threshold selection based on the honey bee mating optimization", ***Expert Systems with Applications***, Vol. 37, No. 6, (2010), 4580-4592.
21. Pal, N. R. and Pal, S. K., "Image model, poisson distribution and object extraction", ***International Journal of Pattern Recognition and Artificial Intelligence***, Vol. 5, No. 03, (1991), 459-483.
22. Lee, S.-K., Lo, C.-S., Wang, C.-M., Chung, P.-C., Chang, C.-I., Yang, C.-W., and Hsu, P.-C., "A computer-aided design mammography screening system for detection and classification of microcalcifications", ***International Journal of Medical Informatics***, Vol. 60, No. 1, (2000), 29-57.
23. Caselles, V., Kimmel, R. and Sapiro, G., "Geodesic active contours", ***International Journal of Computer Vision***, Vol. 22, No. 1, (1997), 61-79.
24. Osher, S. and Fedkiw, R., "Level set methods and dynamic implicit surfaces", Springer, Vol. 153, (2003).
25. Zhao, H.-K., Chan, T., Merriman, B. and Osher, S., "A variational level set approach to multiphase motion", ***Journal of Computational Physics***, Vol. 127, No. 1, (1996), 179-195.

A New Method for Root Detection in Minirhizotron Images: Hypothesis Testing Based on Entropy-based Geometric Level Set Decision

S. V. Shojaedini, M. Heidari

Department of Electrical Engineering, Iranian Research Organization for Science and Technology , Tehran-Iran

P A P E R I N F O

Paper history:
Received 10 June 2013
Received in revised form 27 August 2013
Accepted 14 September 2013

Keywords:
Root Detection
Minirhizotron Images
Hypothesis testing
Entropy
Geometric Level Set

چکیده

در این مقاله روشی جدید به منظور آشکارسازی ریشه‌های گیاهان در تصاویر گرفته شده توسط سیستم مینی رایزوترون ارایه می‌شود. در روش پیشنهادی به منظور تفکیک ریشه‌ها از پس زمینه و نویز موجود در تصاویر، ابتدا مساله با استفاده از مفهوم آزمون فرضها بازتعریف می‌شود. در گام بعدی تابع تصمیمی که با استفاده از سطوح همتراز مبتنی بر آنتروپی تصاویر تعریف می‌شود، محاسبه می‌گردد. مقدار این تابع می تواند فرضیه صحیح را مشخص نموده و لذا ریشه را از پس زمینه و نویز تصاویر تفکیک نماید. عملکرد روش پیشنهادی با استفاده از تصاویر اخذ شده توسط سیستم مینی رایزوترون در دو سناریوی مختلف آزموده می‌شود. در اولین سناریو تصاویر مورد آزمون شامل ریشه هستند، در حالی که سناریوی دوم مربوط به تصاویری است که شامل هیچ ریشه ای نمی باشند. نتایج حاصل از مقایسه عملکرد روش پیشنهادی و چند روش موجود حاکی از برتری روش پیشنهادی این مقاله در استخراج ریشه های صحیح هستند. همچنین نتایج به دست آمده نشان می دهند که به موازات برتری مزبور، روش پیشنهادی این مقاله ریشه‌های نادرست کمتری را نیز نسبت به سایر روش‌های آزموده شده به دست می‌دهد.

doi: *10.5829/idosi.ije.2014.27.01a.12*.